Laminar streaks with spanwise wall forcing

Pierre Ricco
Department of Mechanical Engineering, King's College London, Strand, London WC2R 2LS, United Kingdom

(Received 15 January 2011; accepted 21 April 2011; published online 17 June 2011)

The influence of steady sinusoidal oscillations of spanwise wall velocity on the Klebanoff modes, i.e. unsteady streaky fluctuations induced by free-stream turbulence in the pre-transitional Blasius boundary layer, is investigated numerically. The wall motion induces a spanwise boundary layer which grows downstream as $x^{1/6}$ and has an asymptotic analytical solution at large downstream distances. While the forcing has no effect on the initial growth of the streaks, their intensity eventually increases or decreases substantially depending on the relative magnitude between the forcing wavelength and the characteristic length scales of the streaks. The wall actuation enhances the streak intensity if the streak spanwise length scale is much larger than the Blasius boundary layer thickness. The streak energy is instead attenuated when the spanwise viscous diffusion effects play a key role. Wall pressure fluctuations may also be significantly damped in this case. The Klebanoff modes generated by full-spectrum free-stream turbulence are predicted to be attenuated by the wall motion. The asymptotic scaling analysis reveals that there exists an optimal forcing wavelength for full-spectrum streak attenuation as long as the spanwise length scales of the dominant streaks are as large as or smaller than the Blasius boundary layer thickness, a common scenario encountered in experiments. The optimal forcing wavelength is found to be comparable with the streak streamwise length scale. As the amplitude of the wall forcing increases, the reduction of streak intensity grows monotonically. The streaks are completely suppressed in the limit of large amplitude. © *2011 American Institute of Physics*. [doi:10.1063/1.3593469]

I. INTRODUCTION

One of the central problems in the fluid engineering is that wall-bounded turbulent flows usually exert a much higher wall friction than laminar boundary layers. This impacts negatively on the dynamics of vehicles moving through air and water, on the energetic performances of turbine jet engines, and on the transport of oil and gas through pipelines. Fluid dynamics researchers therefore aim at reducing the friction drag by extending the laminar region through the attenuation of the flow disturbances responsible for laminar-turbulent transition, or by working toward a reduction of the turbulence intensity in order to achieve a lower turbulent wall-shear stress.

An effective method to obtain turbulent drag reduction is to impose uniform time-dependent spanwise wall oscillations, as first shown numerically by Jung *et al*.[1] Experimental[2–4] and numerical[5] studies have reported that the turbulent drag may decrease up to about 45%, and the rms of the turbulent velocity components is strongly reduced during the wall motion. The induced oscillatory boundary layer interferes effectively with the turbulence-producing cycle and damps the bursting and sweeping events in the near-wall region.[6] An optimal boundary layer thickness for drag reduction exists and it corresponds[7] to $T^+ \approx 120$, where T is the period of oscillation and the superscript $+$ denotes the scaling by viscous wall units, i.e. by the wall turbulent friction velocity and the kinematic viscosity of the fluid. Different forms of sinusoidal wall forcing have also been found to alter the turbulent drag. Viotti *et al*.[8] have showed by direct numerical simulations that steady streamwise oscillations of the spanwise wall velocity are more effective for drag reduction than temporal oscillations, while streamwise-traveling waves of the spanwise wall velocity have been associated with both drag reduction and drag increase.[9–11]

Transitional boundary layers modified by near-wall spanwise forcing have instead received a much more limited attention. Sinusoidal wall oscillations have been shown to reduce the growth rate of the most unstable Görtler vortex evolving on a concave surface.[12] However, there is no evidence yet that spanwise forcing can damp the intensity of other common transitional disturbances, such as Tollmien-Schlichting waves, swept-wing cross vortices, or transiently growing streaky structures.[13]

Prompted by the lack of works in this area, in the present paper we study numerically the effects of steady streamwise sinusoidal oscillations of spanwise wall velocity on the Klebanoff modes, namely low-frequency disturbances growing algebraically in pre-transitional boundary layers exposed to free-stream vortical fluctuations. The spanwise length scale of the Klebanoff modes (also referred to as laminar streaks) is typically comparable with the boundary layer thickness, while the streamwise length scale is typically two orders of magnitude larger. The key feature for streak formation and evolution is the direct, continuous action of free-stream vortical perturbations, as evidenced in the theoretical work by Leib *et al*.[14] (hereinafter referred to as LWG99) and by experimental observations.[15] It is believed that small-amplitude streaks evolve linearly, while nonlinear dynamics governs more intense streaks, which may become unstable if exceeding a certain energetic threshold, thus triggering bypass transition to turbulence.[15] Different mechanisms for the streak breakdown have been proposed. Jacobs and Durbin[16] found that the streaks are very stable when they remain near the wall, while they become unstable when they migrate to the upper portion of the boundary layer and interact with vortical structures with smaller scales, which are directly related to free-stream turbulence. Wu and Choudhari[17] recognized the importance of the streak unsteadiness in inducing a near-wall torsion of the velocity profile, which triggers inviscid instability and leads to transition. Brandt[18] instead identified the mutual nonlinear interaction of adjacent streaks as responsible for bypass transition to turbulence.

Since the Klebanoff modes are ubiquitous in numerous technological fluid systems where the external flow is perturbed by free-stream turbulence, it is of crucial importance to be able to control their growth. As previous studies agree on the idea that the streaks are harbingers of bypass transition, an attenuation of streak intensity is bound to postpone transition, therefore leading to friction reduction. Although the whole transition scenario, which is inherently a nonlinear process, is not studied here because the perturbations are assumed of small amplitude with respect to the mean flow (linearized theory), steady wall oscillations are found to be an effective vehicle for suppressing the intensity of the Klebanoff modes. A full nonlinear simulation would have to be performed to verify whether the wall forcing can stop the transition process. The present work is in line with recent research efforts to control the streaks, by wall suction,[19,20] wall cooling,[21] or compliant surfaces.[22]

The adopted mathematical framework is the one by LWG99 and Ricco[23] (hereinafter referred to as R09), modified to account for the action of the spanwise boundary layer engendered by the wall oscillations. The incompressible Navier-Stokes equations are simplified through asymptotic analysis by assuming that the streamwise scale of the streaks is asymptotically larger than the boundary-layer thickness and the spanwise length scale, as found in experimental studies.[15] The resulting unsteady boundary region equations, complemented by rigorous initial and free-stream boundary conditions, are solved numerically.

The mathematical formulation and the numerical procedures are presented in Sec. II. The spanwise mean flow is studied in Sec. III A, while the dynamics of the Klebanoff modes modified by the wall motion is discussed in Sec. III B. A summary is presented in Sec. IV.

II. MATHEMATICAL FORMULATION

A. Scaling

The mathematical framework is based on the works by LWG99 and R09, adapted to include steady sinusoidal spanwise wall motion. We consider a uniform, incompressible flow with velocity U_∞ past an infinitely thin plate. Homogeneous, statistically stationary vortical disturbances are superimposed on the free-stream mean flow and are of the convective gust type, i.e. they are advected at U_∞. The flow is described through a Cartesian coordinate system, i.e. by $\mathbf{x} = x\widehat{\mathbf{i}} + y\widehat{\mathbf{j}} + z\widehat{\mathbf{k}}$, where x, y, and z denote the streamwise, wall-normal, and spanwise directions, scaled by the gust spanwise wavelength λ_z^*. The symbol * indicates a dimensional quantity. The velocities are non-dimensionalized by U_∞ and the pressure by $\rho^* U_\infty^2$, where ρ^* is the density. The free-stream vorticity fluctuations are written as a superposition of sinusoidal disturbances

$$\mathbf{u} - \widehat{\mathbf{i}} = \epsilon \widehat{\mathbf{u}}^\infty e^{i(\mathbf{k}\cdot\mathbf{x} - k_x t)} + c.c.,$$

where $\epsilon \ll 1$ indicates the gust amplitude, $\widehat{\mathbf{u}}^\infty = \{\hat{u}_x^\infty, \hat{u}_y^\infty, \hat{u}_z^\infty\}$ ($|\widehat{\mathbf{u}}^\infty| = 1$), $\mathbf{k} = \{k_x, k_y, k_z\}$, and $c.c.$ is the complex conjugate. We focus on low-frequency disturbances with $k_x \ll k_y, k_z$, as these penetrate the most into the boundary layer to form the laminar streaks. A Reynolds number is defined as $R_\lambda \equiv U_\infty \lambda_z^*/\nu^* \gg 1$. As shown by LWG99, continuity requires that $\mathcal{O}(\epsilon)$ free-stream fluctuations generate $\mathcal{O}(\epsilon/k_x)$ boundary layer streamwise disturbances because the streamwise velocity fluctuations evolve on a much longer length scale than the spanwise velocity fluctuations. We assume that the amplitude of the boundary layer disturbance is much smaller than the order-one mean flow amplitude to linearize the equations. The condition for linearization is therefore $\epsilon/k_x \ll 1$. As the spanwise length scale is comparable with the boundary layer thickness,[15] which are both smaller than the streamwise wavelength of the gust, a distinguished limit is $k_x R_\lambda = \mathcal{O}(1)$. It further follows that the condition for linearization may be written as $\epsilon R_\lambda \ll 1$.

The wall moves along the spanwise direction according to

$$\widetilde{W}_w^* = \widetilde{W}_m^* \sin\left(\frac{2\pi x^*}{\Lambda_x^*}\right).$$

The streamwise wall forcing wavelength Λ_x^* is assumed to be comparable with λ_x^*, so that a parameter $\mathcal{K}_x \equiv \lambda_x^*/\Lambda_x^* = \mathcal{O}(1)$ is defined. The physical domain is shown in Figure 1.

B. The mean flow

The mean flow is described by the steady three-dimensional Navier-Stokes equations. Terms involving partial derivatives along the spanwise direction are null because the flow is independent of this direction. The equations read

$$\frac{\partial U}{\partial x} + \frac{\partial V}{\partial y} = 0, \tag{1}$$

$$U\frac{\partial U}{\partial x} + V\frac{\partial U}{\partial y} = -\frac{\partial P}{\partial x} + \frac{1}{R_\lambda}\frac{\partial^2 U}{\partial x^2} + \frac{1}{R_\lambda}\frac{\partial^2 U}{\partial y^2}, \tag{2}$$

$$U\frac{\partial V}{\partial x} + V\frac{\partial V}{\partial y} = -\frac{\partial P}{\partial y} + \frac{1}{R_\lambda}\frac{\partial^2 V}{\partial x^2} + \frac{1}{R_\lambda}\frac{\partial^2 V}{\partial y^2}, \tag{3}$$

$$U\frac{\partial \widetilde{W}}{\partial x} + V\frac{\partial \widetilde{W}}{\partial y} = \frac{1}{R_\lambda}\frac{\partial^2 \widetilde{W}}{\partial x^2} + \frac{1}{R_\lambda}\frac{\partial^2 \widetilde{W}}{\partial y^2}, \tag{4}$$

where $U(x,y)$, $V(x,y)$, and $\widetilde{W}(x,y)$ represent the mean streamwise, wall-normal, and spanwise velocity components, respectively, and $P(x,y)$ is the mean pressure. The boundary conditions are

$$U(x,0) = V(x,0) = 0, \quad \widetilde{W}(x,0) = \widetilde{W}_w, \quad x > 0,$$

$$U \to 1, \quad \widetilde{W} \to 0 \quad \text{as} \quad y \to \infty.$$

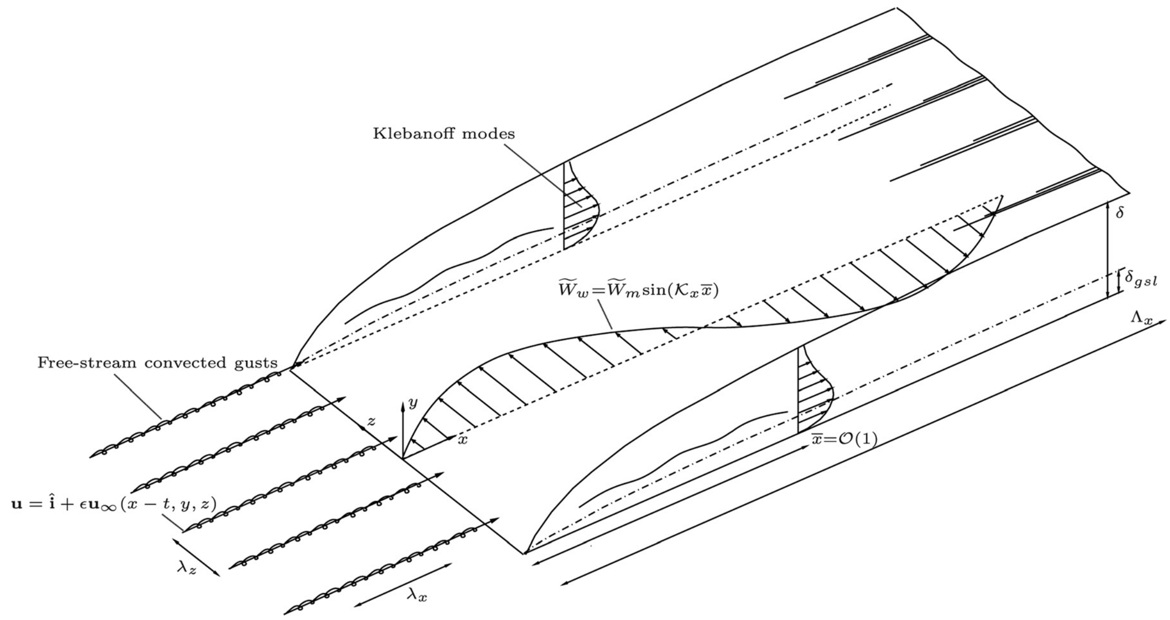

FIG. 1. Schematic of the physical domain.

The continuity x- and y-momentum equations (1), (2), and (3) are independent of the z-momentum equation (4), which proves that the mean flow along (x,y) planes is independent of the spanwise mean flow. In the limit $R_\lambda \gg 1$, Eqs. (1), (2), and (3) reduce to the mean two-dimensional boundary-layer equations with constant pressure, and the solution therefore agrees with the Blasius boundary layer.[24] The similarity variable for the Blasius flow is

$$\eta \equiv y\left(\frac{R_\lambda}{2x}\right)^{1/2} = y^* \sqrt{\frac{U_\infty}{2\nu^* x^*}}.$$

The mean flow solution along (x,y) planes is expressed as

$$U = F'(\eta), \quad V = -(2xR_\lambda)^{-1/2}(F - \eta F'),$$

where the prime indicates differentiation with respect to η. The equation governing F is

$$F''' + FF'' = 0,$$

subject to the boundary conditions

$$F(0) = 0,\ F'(0) = 0,\ \text{and}\ F' \to 1\ \text{and}\ \ \eta \to \infty.$$

The z-momentum equation can be simplified by assuming that the thickness of the viscous spanwise layer δ^*_{gsl} induced by the wall motion is of the same order of magnitude of δ^*, the thickness of the Blasius boundary layer, and by assuming that $\Lambda^*_x \gg \delta^*_{gsl}$. Thanks to the first assumption, the coordinate η can be used in the z-momentum equation (4), while the second assumption allows neglecting the streamwise viscous diffusion with respect to the wall-normal viscous diffusion in Eq. (4). Both hypotheses will be verified by the asymptotic analysis and the numerical calculations in Sec. III A. Furthermore, the streamwise coordinate in Eq. (4) can be scaled by $\lambda^*_x/2\pi$ because $\mathcal{K}_x = \mathcal{O}(1)$, i.e. $\bar{x} = k_x x = 2\pi x^*/\lambda^*_x = \mathcal{O}(1)$. The z-momentum equation (4) can be written as

$$2\bar{x}F'\frac{\partial \widetilde{W}}{\partial \bar{x}} - F\frac{\partial \widetilde{W}}{\partial \eta} = \frac{\partial^2 \widetilde{W}}{\partial \eta^2}. \tag{5}$$

The boundary conditions are $\widetilde{W}(\bar{x},0) = \widetilde{W}_m \sin(\mathcal{K}_x\bar{x})$ and $\widetilde{W} \to 0$ as $\eta \to \infty$. Equation (5) is parabolic along the $\bar{x}$ direction and therefore requires an initial condition as $\bar{x} \ll 1$. In this limit, $\sin(\mathcal{K}_x\bar{x}) \sim \mathcal{K}_x\bar{x}$, which suggests that the initial condition can be $\widetilde{W} = \widetilde{W}_m\mathcal{K}_x\bar{x}\overline{W}(\eta)$, where $\overline{W}(\eta)$ satisfies

$$2F'\overline{W} - F\overline{W}' = \overline{W}'', \tag{6}$$

subject to $\overline{W}(0) = 1$ and $\overline{W} \to 0$ as $\eta \to \infty$. Second-order, implicit finite-difference schemes are employed to solve Eqs. (5) and (6).[25]

C. The disturbance flow

The mean and disturbance flows are written as

$$\{u,v,w,p\} = \{U,V,\widetilde{W},-1/2\} + \epsilon\left\{\bar{u}_0(\bar{x},\eta), \left(\frac{2\bar{x}k_x}{R_\lambda}\right)^{1/2}\bar{v}_0(\bar{x},\eta), \bar{w}_0(\bar{x},\eta), \bar{p}_0(\bar{x},\eta)\right\} \times e^{i(k_z z - k_x t)} + c.c. + \cdots$$

The velocity and pressure disturbances are[26]

$$\left.\begin{aligned}
\{\bar{u}_0,\bar{v}_0\} &= C^{(0)}\{\bar{u}^{(0)},\bar{v}^{(0)}\} + (ik_z/k_x)C\{\bar{u},\bar{v}\},\\
\bar{w}_0 &= -(ik_x/k_z)C^{(0)}\bar{w}^{(0)} + C\bar{w},\\
\bar{p}_0 &= (k_x/R_\lambda)C^{(0)}\bar{p}^{(0)} + i\kappa_z(k_x/R_\lambda)^{1/2}C\bar{p},
\end{aligned}\right\} \tag{7}$$

where $\kappa_z \equiv k_z/(k_xR_\lambda)^{1/2} = \sqrt{2\pi\nu^*\lambda^*_x/U_\infty}/\lambda^*_z = \mathcal{O}(1)$ is a measure of the ratio between the spanwise and wall-normal viscous diffusion effects (LWG99), $C^{(0)} \equiv \hat{u}^\infty_x + ik_x\hat{u}^\infty_y/\Gamma$, $C \equiv \hat{u}^\infty_z + ik_z\hat{u}^\infty_y/\Gamma$, and $\Gamma \equiv \sqrt{k_x^2 + k_z^2}$.

The focus is on streamwise locations where the spanwise viscous diffusion is of the same order as that in the wall-normal direction, i.e. where $\delta^* = \mathcal{O}(\lambda_z^*)$ or $x/R_\lambda = \mathcal{O}(1)$. The linearized three-dimensional unsteady boundary-region (LUBR) equations describe the disturbance dynamics. They are the asymptotically rigorous limit of the Navier-Stokes equations for disturbances with $k_x^*/k_z^* \to 0$ at $\bar{x} = \mathcal{O}(1)$, i.e. with a streamwise wavelength which is long with respect to the boundary-layer thickness and the spanwise wavelength. In this limit, the first-order terms in Eq. (7) are proportional to $\{\bar{u}, \bar{v}, \bar{w}, \bar{p}\}$, while the second-order terms, i.e. $\mathcal{O}(k_x^*/k_z^*)$ smaller than the leading-order ones, are the ones proportional to $\{\bar{u}^{(0)}, \bar{v}^{(0)}, \bar{w}^{(0)}, \bar{p}^{(0)}\}$. The LUBR equations are suited for studying the laminar streaks because the experimental data[15] indicate that these structures are streamwise-elongated and their spanwise wavelength is $\mathcal{O}(\delta^*)$. Both $\{\bar{u}, \bar{v}, \bar{w}, \bar{p}\}$ and $\{\bar{u}^{(0)}, \bar{v}^{(0)}, \bar{w}^{(0)}, \bar{p}^{(0)}\}$ satisfy the LUBR equations

$$\frac{\partial \bar{u}}{\partial \bar{x}} - \frac{\eta}{2\bar{x}}\frac{\partial \bar{u}}{\partial \eta} + \frac{\partial \bar{v}}{\partial \eta} + \bar{w} = 0, \tag{8}$$

$$\left(-i + \kappa_z^2 - \frac{\eta F''}{2\bar{x}} + iW\right)\bar{u} + F'\frac{\partial \bar{u}}{\partial \bar{x}} - \frac{F}{2\bar{x}}\frac{\partial \bar{u}}{\partial \eta} - \frac{1}{2\bar{x}}\frac{\partial^2 \bar{u}}{\partial \eta^2} + F''\bar{v} = 0, \tag{9}$$

$$\left(-i + \kappa_z^2 + \frac{(\eta F')'}{2\bar{x}} + iW\right)v + F'\frac{\partial \bar{v}}{\partial \bar{x}} - \frac{F}{2\bar{x}}\frac{\partial \bar{v}}{\partial \eta} - \frac{1}{2\bar{x}}\frac{\partial^2 \bar{v}}{\partial \eta^2} - \frac{\eta(\eta F')' - F}{(2\bar{x})^2}\bar{u} + \frac{1}{2\bar{x}}\frac{\partial \bar{p}}{\partial \eta} = 0, \tag{10}$$

$$\left(i\frac{\partial W}{\partial \bar{x}} - \frac{i\eta}{2\bar{x}}\frac{\partial W}{\partial \eta}\right)\bar{u} + i\frac{\partial W}{\partial \eta}v + \left(-i + \kappa_z^2 + iW\right)\bar{w} + F'\frac{\partial \bar{w}}{\partial \bar{x}} - \frac{F}{2\bar{x}}\frac{\partial \bar{w}}{\partial \eta} - \frac{1}{2\bar{x}}\frac{\partial^2 \bar{w}}{\partial \eta^2} - \kappa_z^2\bar{p} = 0, \tag{11}$$

where $W = k_z\widetilde{W}/k_x = \mathcal{O}(1)$, which shows that $V = \mathcal{O}(\widetilde{W})$ and $\widetilde{W} \ll U$. At the wall, the no-slip wall boundary conditions apply to all the velocity components in Eq. (7). The boundary conditions as $\eta \to \infty$ are identical to (2.13), (2.17), and (2.21)-(2.26) at pages 276-278 in R09 because the large-η equations (5.16)-(5.19) in LWG99 are unvaried as the spanwise mean flow vanishes as $\eta \to \infty$ and because of the assumption $\delta_{gsl}^*/\delta^* = \mathcal{O}(1)$. Therefore, $\widetilde{W}$ does not influence the outer disturbance flow (in Sec. III A, it is shown that the numerical value of δ_{gsl}^* is smaller than δ^* for all the flow conditions tested). The initial conditions at $\bar{x} \ll 1$ are identical to the ones in Sec. 2.1.2 in R09 because the terms involving W are of higher order. Equations (8)–(11) are solved by marching downstream through a second-order, implicit finite-difference scheme employing a grid with a uniform wall-normal mesh size $\Delta\eta = 0.03$ and a streamwise step size $\Delta\bar{x} = 5 \times 10^{-4}$. The domain extends up to $\eta = 30$. More details on the computational procedures are found in R09.

III. RESULTS

A. The spanwise mean flow

The spanwise mean flow W described by Eq. (5) is studied in this section. Figure 2 displays profiles of $W(\bar{x}, \eta)$ for $W_m = 1$ and $\mathcal{K}_x = 5$ at locations $\bar{x}$ along the first wavelength of wall forcing (top graph) and along the 50th wavelength of wall forcing (bottom graph). The top graph clearly shows that, although the wall forcing is sinusoidal, the spanwise velocity at fixed non-zero η is not so along the first wavelength. It is also found that the spanwise boundary layer is thinner than the Blasius boundary layer. Further downstream (bottom graph), the spanwise boundary layer becomes even

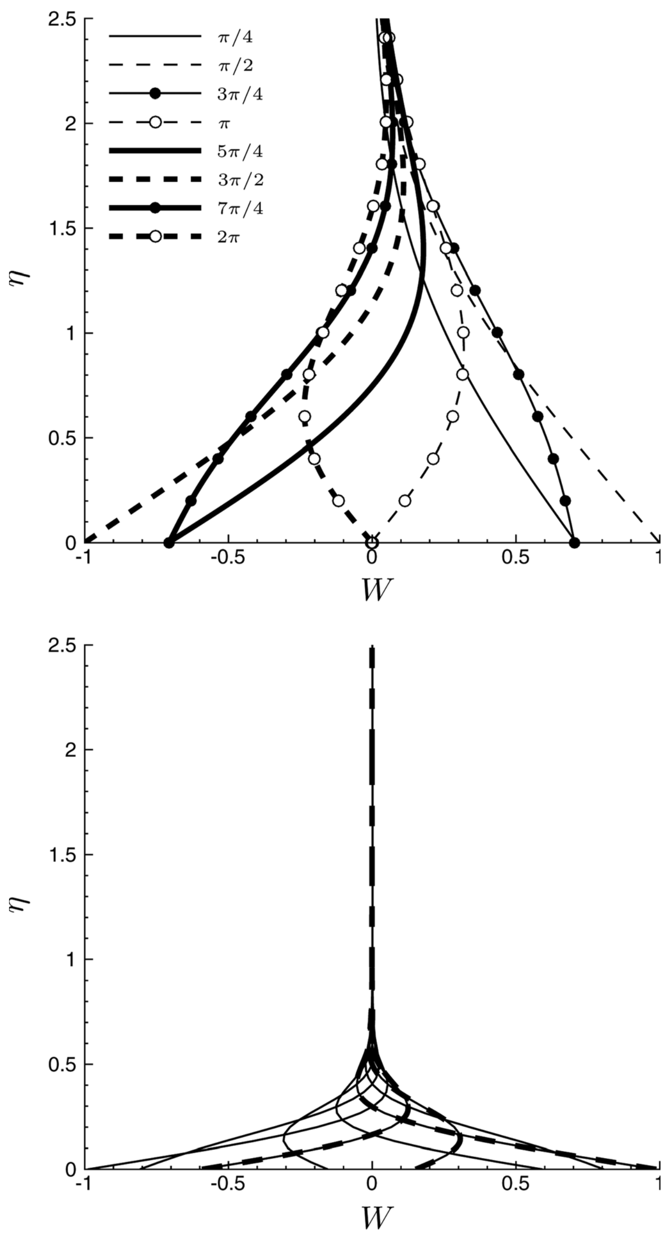

FIG. 2. Profiles of spanwise mean flow $W(\bar{x}, \eta)$ for $W_m = 1$ and $\mathcal{K}_x = 5$. Top: $0 < \bar{x} < 2\pi/\mathcal{K}_x$; the numbers in the legend indicate the phase of wall motion. Bottom: $49 \cdot 2\pi/\mathcal{K}_x < \bar{x} < 50 \cdot 2\pi/\mathcal{K}_x$; solid lines denote the full numerical solution, and the dashed lines indicate the asymptotic solution (13) for $\bar{x} \gg 1$.

thinner than the Blasius layer and the motion tends to become sinusoidal along η-constant planes.

As $\bar{x} \gg 1$, Eq. (5) can be suitably simplified and an analytical solution can be found in terms of Airy function of the first kind (see Abramowitz and Stegun[27] at page 446). In this limit, the spanwise boundary layer is much thinner than the Blasius boundary layer. It follows that the Blasius flow may be suitably represented as $F' = \lambda_b \eta + \mathcal{O}(\eta^2)$ and $F = \mathcal{O}(\eta^2)$, where $\lambda_b = F''(0) \approx 0.4696$. Also, as $\bar{x}$ varies only slightly along one wavelength of wall forcing, the value of $\bar{x}$ in the first term on the left hand side of Eq. (5) can be taken as constant, $\bar{x} \approx \bar{x}_0$. Equation (5) therefore becomes

$$2\bar{x}_0 \lambda_b \eta \frac{\partial \widetilde{W}}{\partial \bar{x}} = \frac{\partial^2 \widetilde{W}}{\partial \eta^2}. \qquad (12)$$

As the coefficients in Eq. (12) are independent of $\bar{x}$, one can assume $\widetilde{W} = \widetilde{W}_m \Im\left[\widehat{W}(\eta)\exp(i\mathcal{K}_x\bar{x})\right]$, where $\Im$ indicates the imaginary part. The change of variable $\widehat{\eta} = (2i\mathcal{K}_x\bar{x}_0\lambda_b)^{1/3}\eta$ leads to the Airy equation $\widehat{W}'' = \widehat{\eta}\widehat{W}$, subject to $\widehat{W} \to 0$ as $\eta \to \infty$ and $\widehat{W}(0) = 1$. The solution is $\widehat{W} = \mathrm{Ai}(\widehat{\eta})/\mathrm{Ai}(0)$. The asymptotic solution for the spanwise mean flow as $\bar{x} \gg 1$ is thus

$$\widetilde{W} = \widetilde{W}_m \Im\left\{[\mathrm{Ai}(0)]^{-1}\mathrm{Ai}\left[(2i\mathcal{K}_x\bar{x}_0\lambda_b)^{1/3}\eta\right]\exp(i\mathcal{K}_x\bar{x})\right\}. \qquad (13)$$

The excellent agreement between the asymptotic solution (13) (dashed lines) and the numerical solution of Eq. (5) (solid lines) is shown in the bottom graph of Figure 2. As the Blasius layer changes more and more gradually as $\bar{x}$ increases, the spanwise flow resembles the generalized Stokes layer induced by steady streamwise wall oscillations beneath a laminar Poiseuille flow, studied by Viotti *et al.*[8]

The thickness δ^*_{gsl} of the spanwise boundary layer can be estimated through scaling analysis of the steady z-momentum equation. By scaling x^* by Λ^*_x, y^* by δ^*_{gsl}, and by expressing $U^* \approx \tau^* y^*$ (where $\tau^* \equiv \partial U^*/\partial y^*|_{y^*=0}$), the balance between the inertia term driven by the Poiseuille flow and the wall-normal viscous diffusion term leads to δ^*_{gsl} $\mathcal{O}[(\nu^*\Lambda^*_x/\tau^*)^{1/3}]$. As $\tau^* = \mathcal{O}[U_\infty^{3/2}/(\nu^* x^*)^{1/2}]$, it follows that

$$\delta^*_{gsl} = \mathcal{O}\left[\left(\frac{\nu^*}{U_\infty}\right)^{1/2}\Lambda_x^{*1/3}x^{*1/6}\right].$$

As $\delta^* = \mathcal{O}[(x^*\nu^*/U_\infty)^{1/2}]$,

$$\delta_{gsl} = \mathcal{O}\left[(\mathcal{K}_x\bar{x})^{-1/3}\right], \qquad (14)$$

where δ_{gsl} is expressed in η units. It also follows that the streamwise diffusion term in Eq. (4) can be legitimately neglected at $x^* = \mathcal{O}(\Lambda^*_x)$ if $\Lambda^*_x U_\infty/\nu^* \gg 1$ or at $x^* = \mathcal{O}(\lambda^*_x)$ if $\mathcal{K}_x \ll (k_x/R_\lambda)^{1/4}$, which is largely verified because $\mathcal{K}_x = \mathcal{O}(1)$ and k_x^{-1}, $R_\lambda \gg 1$. Expression (14) confirms the numerical result in Figure 2 of the spanwise boundary layer becoming thinner and thinner than the Blasius boundary layer as $\bar{x}$ grows. This is further verified in Figure 3, which shows $\delta_{gsl} = \delta_{gsl}(\bar{x})$ for different $\mathcal{K}_x$ (top graph) and

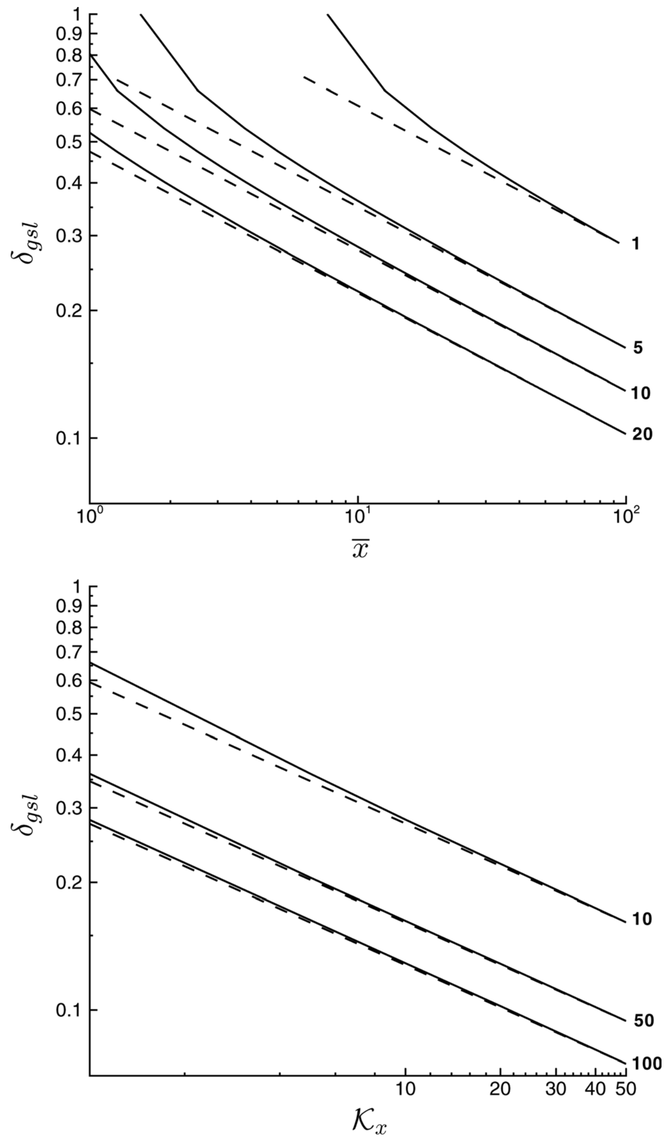

FIG. 3. The δ_{gsl} values (expressed in η units) for $W_m = 1$. Top: The numbers indicate $\mathcal{K}_x$ and the dashed lines denote $\delta_{gsl} = A\bar{x}^{-1/3}$, where the constant A is computed by fitting the numerical results at $\bar{x} = 100$. Bottom: The numbers indicate $\bar{x}$ and the dashed lines denote $\delta_{gsl} = A\mathcal{K}_x^{-1/3}$, where the constant A is computed by fitting the numerical results at $\mathcal{K}_x = 50$.

$\delta_{gsl} = \delta_{gsl}(\mathcal{K}_x)$ for different $\bar{x}$ (bottom graph). The numerical value of δ_{gsl} (solid lines) at each wall forcing wavelength is computed as the η location where the maximum spanwise velocity W along that wavelength equals $\exp(-1)W_m$. The asymptotic trends (dashed lines) are given by Eq. (14), where the constant of proportionality is computed by fitting the asymptotic trend with the numerical result at the last computed $\bar{x}$ location (for the top graph) and for the last computed $\mathcal{K}_x$ (for the bottom graph). The agreement between the asymptotic and the numerical trends is good and it improves as $\bar{x}$ grows. This is expected because expression (14) is found through the assumption $U^* \approx \tau^* y^*$, which provides a better representation of the Blasius flow as δ_{gsl} becomes thinner. The other reason for the improved agreement at large $\bar{x}$ resides in the computation of δ_{gsl}. The numerical calculation gives an average δ_{gsl} along the span of a wavelength because the maximum velocity at fixed η is computed along such

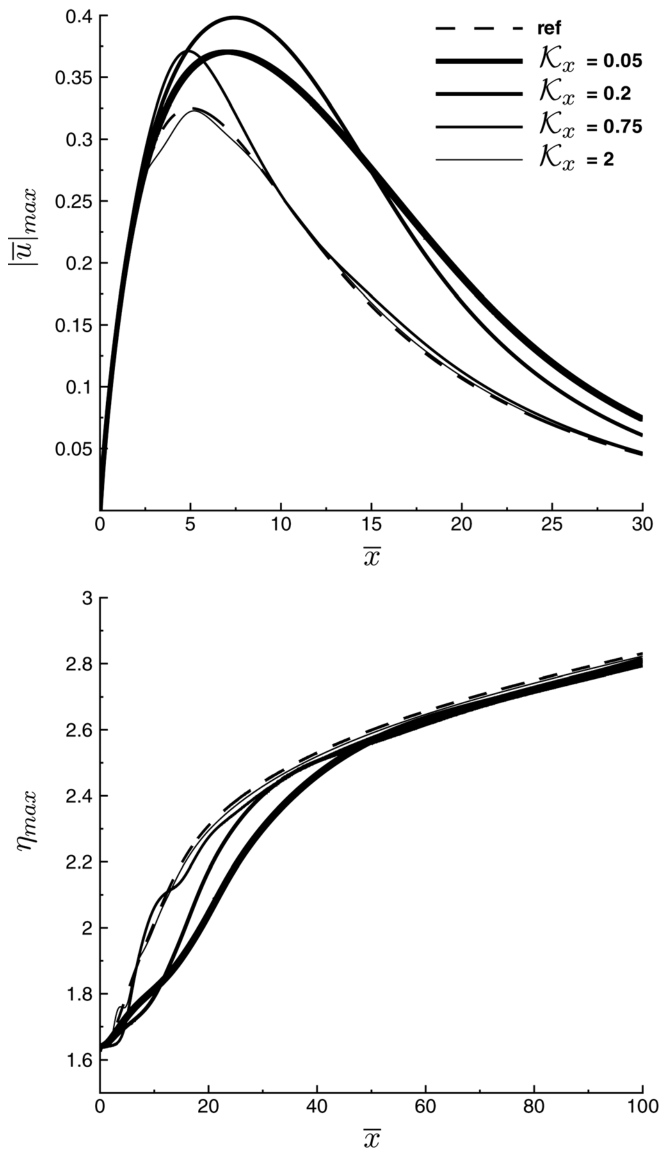

FIG. 4. Top: Downstream evolution of $|\bar{u}|_{\max}$, the maximum (along η) of $|\bar{u}|$, for $\kappa_z = \kappa_y = 0.25$, and $\widetilde{W}_m = 0.16$ at different $\mathcal{K}_x$ (ref denotes case without wall forcing). Bottom: Downstream evolution of η_{max}, the wall-normal location of $|\bar{u}|_{\max}$.

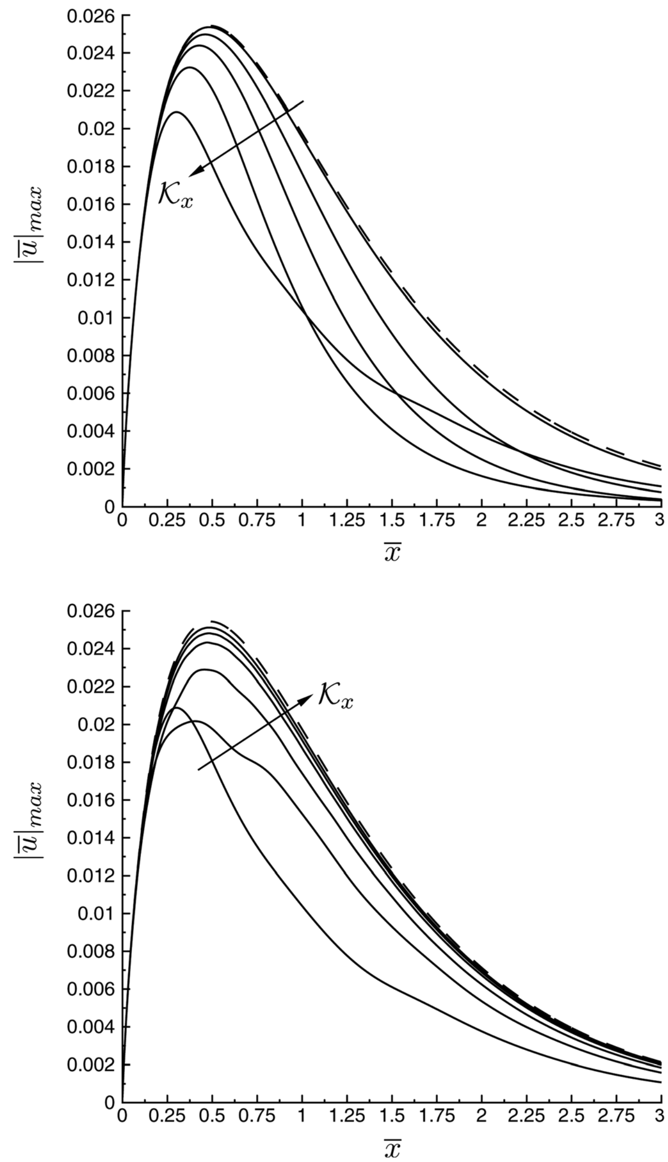

FIG. 5. Downstream evolution of $|\bar{u}|_{\max}$ for $\kappa_z = \kappa_y = 1$ and $\widetilde{W}_m = 0.16$ at different $\mathcal{K}_x$. Dashed lines indicate case without wall forcing. Top: $\mathcal{K}_x = 0.1,\ 0.5,\ 1,\ 2,$ and 5. Bottom: $\mathcal{K}_x = 5,\ 10,\ 20,$ and 50.

distance. However, as verified in Figure 2, during the first wavelengths, the spanwise velocity is not sinusoidal along η-constant planes. The behaviour becomes progressively more sinusoidal as $\bar{x}$ grow, as confirmed in Figure 2 by the agreement between the Airy solution (13) and the numerical results. Therefore, the numerically computed (averaged along one wavelength) δ_{gsl} becomes a better representation of the wall-normal diffusion effects at large $\bar{x}$.

B. Laminar streaks with spanwise wall oscillations

The laminar streaks modified by spanwise wall oscillations are studied in this section. The effect of the two oscillation parameters, $\mathcal{K}_x$ and $\widetilde{W}_m$, is investigated at different κ_z. The Reynolds number $R_\lambda = 394.8$ is the same as the one used by R09 for fixed-wall conditions. As R_λ is fixed, varying κ_z corresponds to changing the frequency k_x. Free-stream gusts of equal spanwise and wall-normal (λ_y^*) wavelengths are considered, so that the non-dimensional parameter $\kappa_y \equiv k_y/(k_x R_\lambda)^{1/2} = \sqrt{2\pi\nu^* \lambda_x^*/U_\infty}/\lambda_y^*$, appearing in the outer boundary conditions (2.13), (2.17), and (2.21)-(2.26) at pages 276-278 in R09, is equal to κ_z. The streaks are therefore generated by axial-symmetric free-stream vortices, a scenario often encountered in wind-tunnel tests where the free-stream turbulence is composed primarily by vortical structures generated by upstream grids of equally spaced bars.[15]

1. Downstream evolution of streaks

The downstream evolution of the maximum (along η) of the streamwise velocity $|\bar{u}|$ and its position η_{max} are presented in Figure 4 for $\kappa_z = 0.25$, and in Figures 5 and 6 for $\kappa_z = 1$, for $\widetilde{W}_m = 0.16$ and different $\mathcal{K}_x$. The streamwise velocity component $\bar{u}$ is chosen as it is dominant in the core of

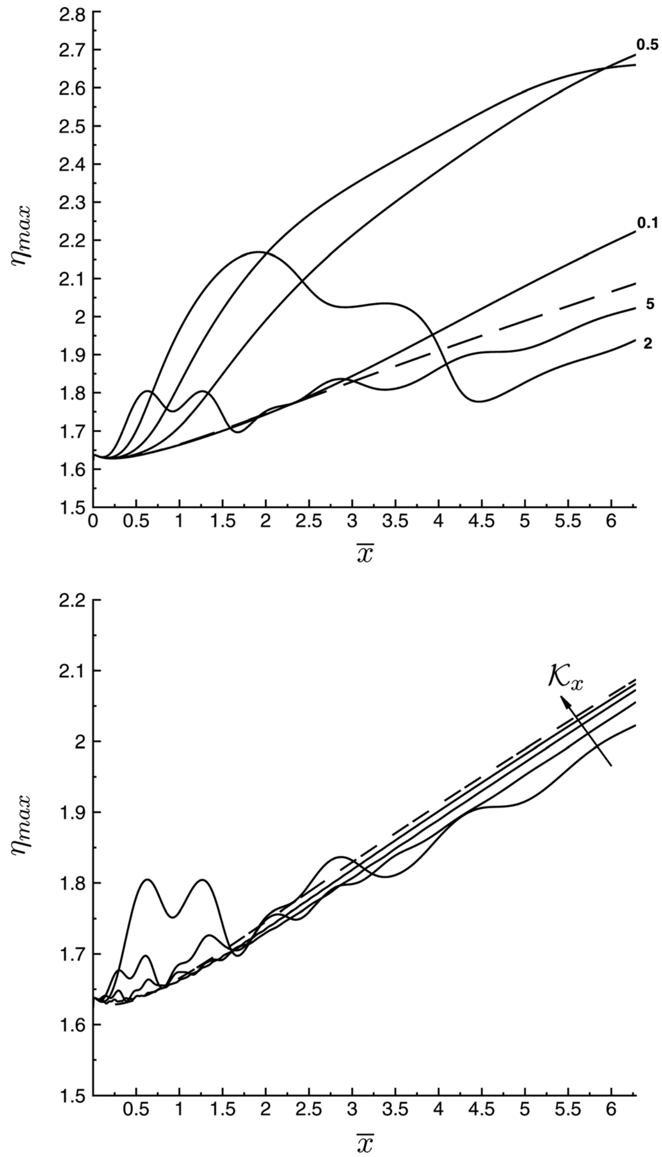

FIG. 6. Downstream evolution of η_{max} for $\kappa_z = \kappa_y = 1$, and $\widetilde{W}_m = 0.16$ at different $\mathcal{K}_x$. Dashed lines indicate case without wall forcing. Top: numbers denote $\mathcal{K}_x$. Bottom: $\mathcal{K}_x = 5,\ 10,\ 20,$ and 50.

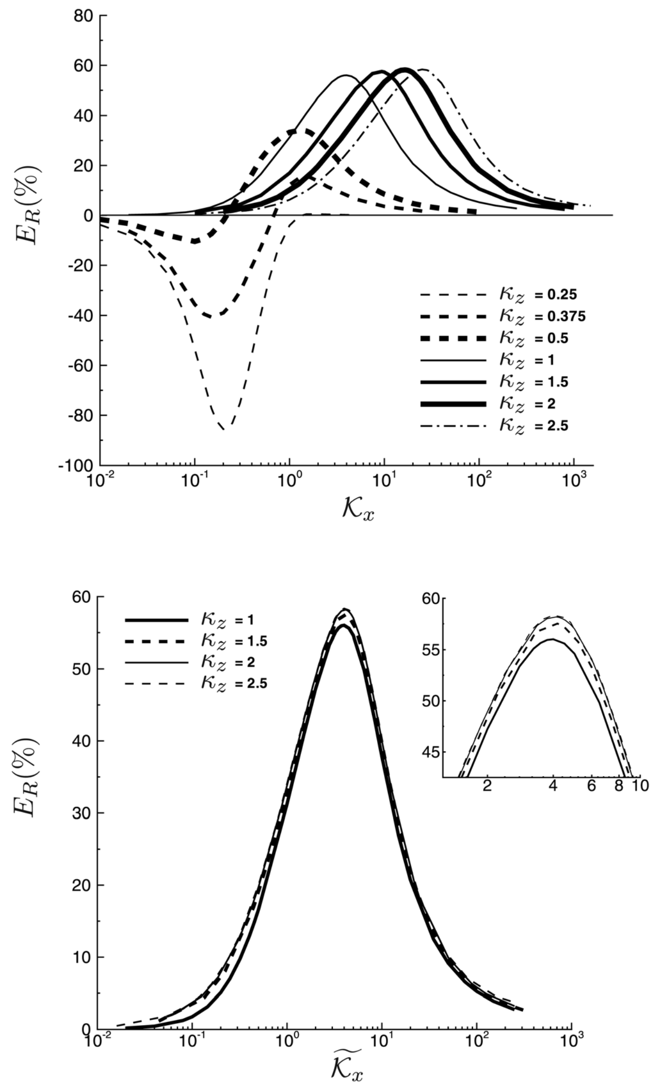

FIG. 7. Top: Percent reduction of streak kinetic energy $E_R(\%)$ as function of $\mathcal{K}_x$ for different κ_z and $\widetilde{W}_m = 0.16$. Bottom: $E_R(\%)$ as function of $\widetilde{\mathcal{K}_x} = \mathcal{K}_x/\kappa_z^2$ for $\kappa_z = 1,\ 1.5,\ 2,$ and 2.5. Inset shows zoom on peak values.

the boundary layer.[23] Figure 4 (top) shows that, for $\kappa_z = 0.25$, the streak amplitude increases with wall oscillations and the maximum amplification is for $\mathcal{K}_x \approx 0.2$. At $\bar{x} \approx 12$, the streamwise velocity is amplified by about a third. In Figure 4 (bottom), the peak of the disturbance is brought closer to the wall up to $\bar{x} \approx 40$, while no effect of the wall forcing is detected farther downstream, i.e. where the streaks show substantial viscous decay.

For $\kappa_z = 1$, the streak amplitude is instead strongly attenuated and the optimal forcing wavelength parameter is $\mathcal{K}_x \approx 5$, as shown in Figure 5. The streamwise velocity may decrease by half at $\bar{x} \approx 1$. For $\mathcal{K}_x$ smaller than the optimal value and for location where the streak intensity is not attenuated by viscous effects ($\bar{x} < 4$), the location of the peak shifts closer to the free stream, as seen in Figure 6. The peak moves much less for $\mathcal{K}_x$ higher than the optimal value. The same effects are found at higher κ_z (not shown). There is no influence of the wall forcing on the initial development of the Klebanoff modes, i.e. up to $\bar{x} \approx 2.5$ for $\kappa_z = 0.25$ and up to $\bar{x} \approx 0.15$ for $\kappa_z = 1$.

2. Global energy of streaks

The effect of wall forcing on the total kinetic energy of the streaks is investigated. A good estimate of such quantity is the integral of the square of the streamwise velocity amplitude $|\bar{u}|$ along the $(\bar{x}, \eta)$ plane because this is the velocity component that dominates within the boundary layer. The energy E is defined as

$$E(\kappa_z, \mathcal{K}_x, \widetilde{W}_m) \equiv \int_0^\infty \int_0^\infty |\bar{u}(\bar{x}, \eta; \kappa_z, \mathcal{K}_x, \widetilde{W}_m)|^2 \mathrm{d}\bar{x}\mathrm{d}\eta. \quad (15)$$

The quantity E in Eq. (15) attains a finite value because $|\bar{u}|$ is null at the wall (no-slip condition) and as $\bar{x} \ll 1$ (refer to (5.25) at page 182 in LWG99), and because it decays rapidly

TABLE I. Flow conditions for available experimental data and optimal wall forcing wavelength given by Eq. (16) for $\widetilde{W}_m = 0.16$.

Researchers	Fluid	λ_z^* (m)	$\Lambda_{x,opt}^*$ (m)
Westin *et al*. (Ref. 28)	Air	0.006	0.76
Watmuff (Ref. 29)	Air	0.01	2.65
Matsubara and Alfredsson (Ref. 15)	Air	0.008	0.98
		0.0075	1.15
Inasawa *et al*. (Ref. 30)	Water	0.015	0.96
Mans *et al*. (Ref. 31)	Water	0.008	0.28
Mans *et al*. (Ref. 32)	Water	0.015	1.02
Zhigulev *et al*. (Ref. 33)	Air	0.0011	0.025
		0.0027	0.149
		0.0016	0.105
		0.0027	0.298

to zero as $\bar{x} \to \infty$ due to viscous effects and as $\eta \to \infty$, as shown by (2.13) in R09. The interest is in $E_R(\%)$, the percent change of E due to the wall oscillation,

$$E_R(\%) = 100 \cdot \frac{E_{fixed} - E_{oscill}}{E_{fixed}},$$

where the subscripts *fixed* and *oscill* refer to the fixed-wall and the oscillating-wall conditions, respectively.

Figure 7 (top) shows $E_R(\%)$ as function of $\mathcal{K}_x$ for $0.25 \le \kappa_z \le 2.5$ and $\widetilde{W}_m = 0.16$. At $\kappa_z = 0.25$, the global kinetic energy is intensified for all $\mathcal{K}_x$ and the optimal value is $\mathcal{K}_x = 0.2$, which confirms the result in Sec. III B 1. For $0.25 < \kappa_z < 1$, disturbances are amplified for low values of $\mathcal{K}_x$ and attenuated at high value of $\mathcal{K}_x$. For $\kappa_z \ge 1$, the wall forcing brings about a reduction of kinetic energy for all forcing conditions.

The trends for $\kappa_z \ge 1$ show very similar shapes and shift toward higher values of $\mathcal{K}_x$ as κ_z grows. Physically, this may be interpreted that at fixed Reynolds number R_λ, as the frequency of the free-stream gust decreases (as κ_z increases), the optimal wavelength of wall forcing becomes smaller and smaller than the streamwise wavelength of the free-stream gust. In the limit $\kappa_z \gg 1$ and $\kappa_y/\kappa_z = \mathcal{O}(1)$, LWG99 found an asymptotic scaling $\bar{u} = \tilde{u}(\tilde{x}, \eta; \kappa_y/\kappa_z)/\kappa_z^2$, $\tilde{x} = \kappa_z^2\bar{x}$, where $\tilde{u}$ satisfies the steady boundary region equations. LWG99's numerical calculations in fact revealed that this scaling is good even for $\kappa_z = 1$. This result also applies to spanwise forcing conditions, which allows the boundary condition for the spanwise wall velocity to be written as $\widetilde{W}_w = \widetilde{W}_m \sin(\widetilde{\mathcal{K}}_x\tilde{x})$, where $\widetilde{\mathcal{K}}_x = \mathcal{K}_x/\kappa_z^2 = \mathcal{O}(1)$. Figure 7 (bottom), where the data in Figure 7 (top) for $\kappa_z \ge 1$ are plotted as function of $\widetilde{\mathcal{K}}_x$, confirms the asymptotic scaling. The agreement is already very good for $\kappa_z = 1$, and the trends for $\kappa_z = 2$ and $\kappa_z = 2.5$ collapse onto each other. The inset shows the peak values more clearly. The optimal forcing parameter is $\widetilde{\mathcal{K}}_x = 4$ for $\widetilde{W}_m = 0.16$.

As amply discussed in LWG99, Klebanoff modes characterised by $\kappa_z = 1$ or higher are likely to dominate a pre-transitional boundary layer perturbed by free-stream turbulence because this range of κ_z corresponds to streaks which are of low frequency and with a typical spanwise length scale which is comparable with the boundary layer thickness. It is therefore likely that the asymptotic scaling discussed above applies to experimental data, such as the ones by Westin *et al*.[28] and Matsubara and Alfredsson.[15]

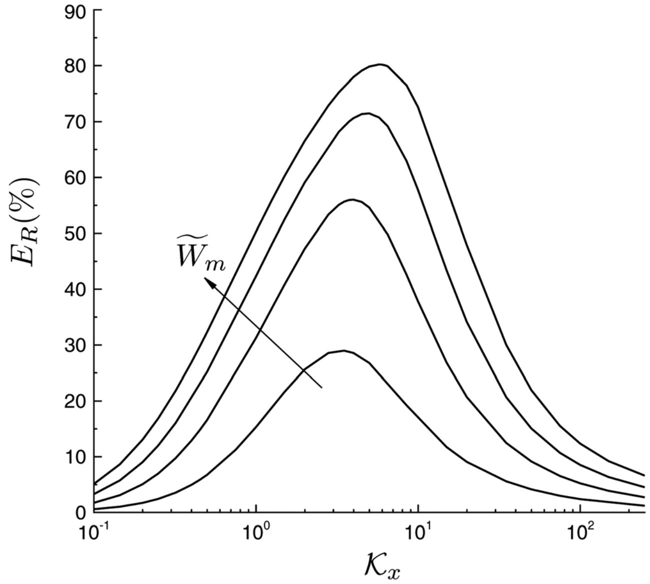

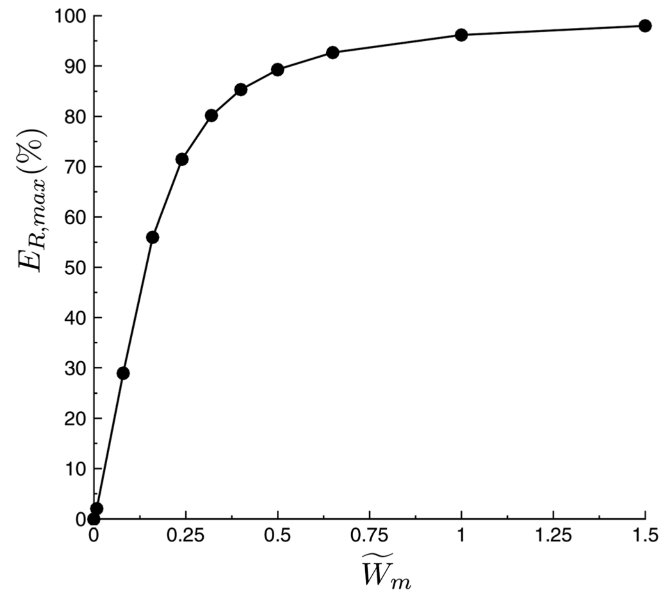

FIG. 8. Top: Percent reduction of streak kinetic energy E_R (%) as function of $\mathcal{K}_x$ for $\kappa_z = 1$ and $\widetilde{W}_m = 0.08$, 0.16, 0.24, and 0.36. Bottom: values of $\mathcal{K}_x$ for maximum of E_R (%) as function of $\widetilde{W}_m$ for $\kappa_z = 1$.

Furthermore, as $\widetilde{\mathcal{K}}_x = \lambda_z^{*2}U_\infty/(2\pi\Lambda_x^*\nu^*)$, it is thus possible to estimate the optimal Λ_x^* for streak attenuation by assuming that λ_z^* is representative of the spanwise length scale of full-spectrum streaks. This latter assumption is supported by the flow visualizations and velocity correlation analysis carried out by Matsubara and Alfredsson,[15] which clearly show that the streaks are characterised by a well-defined spanwise length scale. As the optimal forcing parameter is $\widetilde{\mathcal{K}}_x = 4$ for $\widetilde{W}_m = 0.16$, the optimal streamwise length scale of the wall forcing is thus

$$\Lambda_{x,opt}^*(\text{m}) = \frac{U_\infty\lambda_z^{*2}}{8\pi\nu^*}. \tag{16}$$

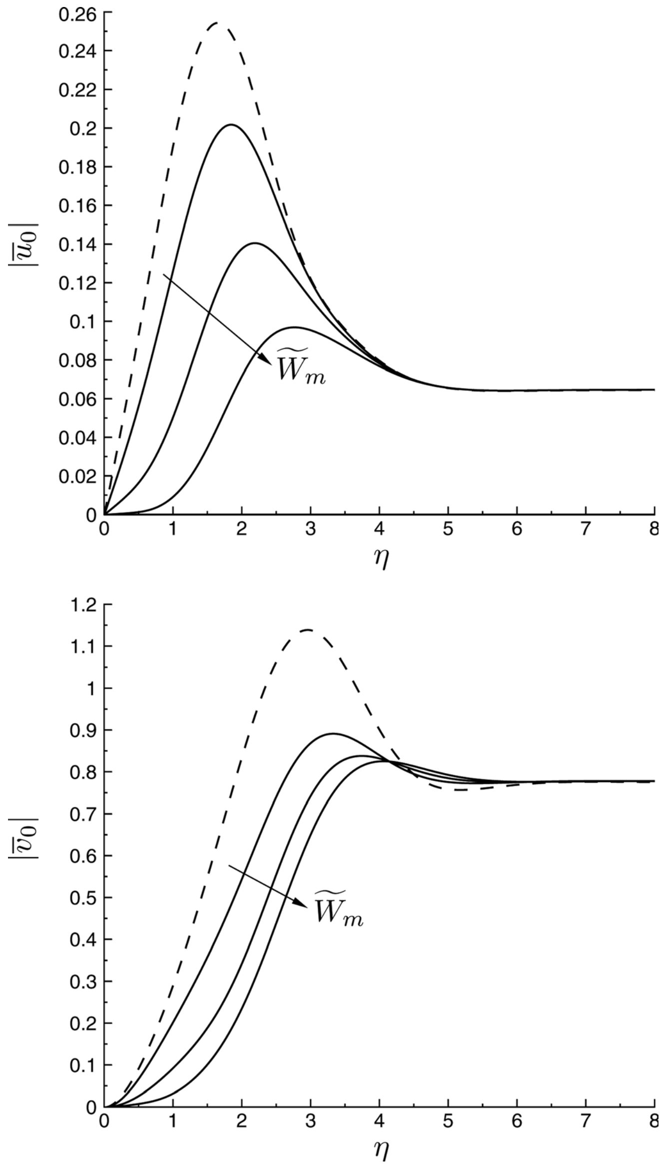

FIG. 9. Streamwise (top) and wall-normal (bottom) velocity profiles for fixed-wall (dashed line) and oscillating-wall conditions (solid lines) at $\bar{x} = 1.18$ for $\kappa_z = \kappa_y = 1$, $\mathcal{K}_x = 0.1$, and $\hat{u}_3^\infty = -0.2$ and for wall forcing conditions $\mathcal{K}_x = 2$ and $\widetilde{W}_m = 0.08,\ 0.16,$ and 0.32.

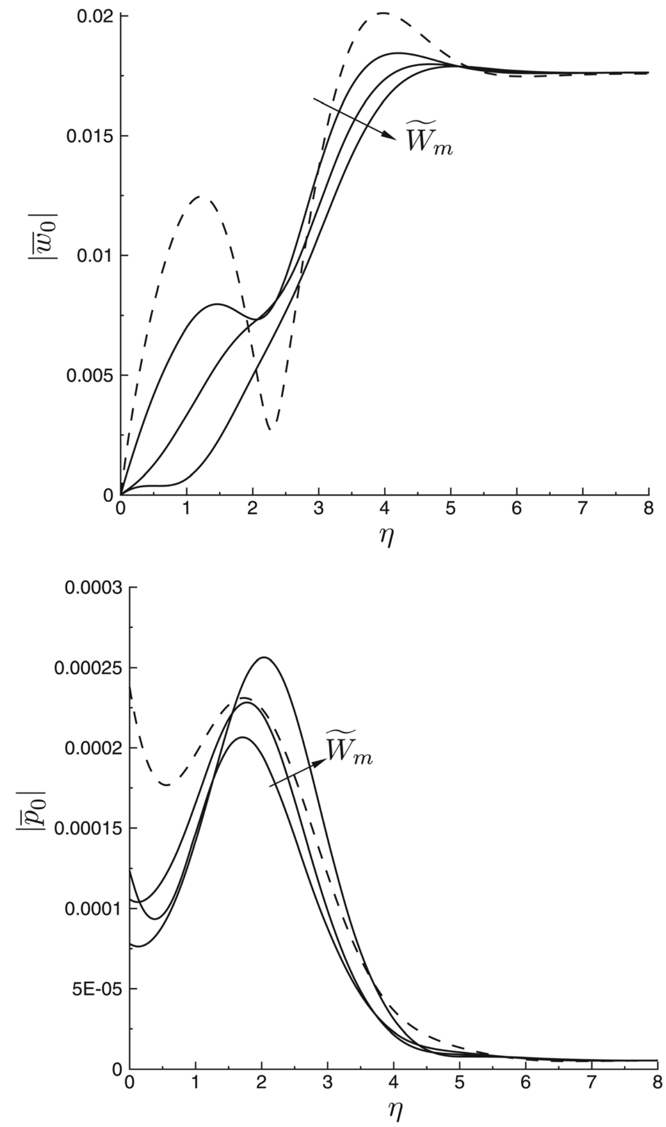

FIG. 10. Spanwise velocity (top) and pressure (bottom) profiles at the same locations and for the same flow conditions of Figure 9.

Table I gives the estimated optimal wall forcing wavelength for the experimental investigations which provide information on the streak spanwise wavelength. The common feature is that $\Lambda^*_{x,opt}$ is much larger than the spanwise length scale of the streaks. For most experiments, the optimal wavelength can be of the order of a meter, so even one hundred times larger than the spanwise wavelength.

It further follows that $\Lambda^*_{x,opt}$ is comparable with the characteristic streamwise length scales of the streaks as it has been amply documented by the experimental studies based on velocity correlations and flow visualizations[15,28] that the streamwise length scale can be even two order of magnitude larger than both the spanwise length scale and the boundary layer thickness (see also R09 for further theoretical discussion on the wind-tunnel data by Westin *et al.*[28]). This scenario bears analogy with the near-wall turbulent flow modified by streamwise steady oscillations studied by Viotti *et al.*[8] For that flow, the optimal wavelength for maximum turbulence attenuation matches the characteristic streamwise length scale of the turbulent low-speed streaks, i.e. $\lambda^+ = 1000$.

Figure 8 (top) shows that, for $\kappa_z = 1$, the streak intensity decreases monotonically as $\widetilde{W}_m$ increases, a behaviour also shared by the reduction of turbulence intensity through wall traveling waves of spanwise velocity[9] and spanwise wall oscillations.[7] The maximum E_R is 89.5% for $\widetilde{W}_m = 0.5$, 96% for $\widetilde{W}_m = 1$, and the energy is eventually completed damped at high $\widetilde{W}_m$. This result can be predicted by dividing each term of Eq. (9) by W and by taking the limit $W \gg 1$. This behaviour also occurs for higher values of κ_z because of the asymptotic scaling displayed in Figure 7. The $\mathcal{K}_x$ value corresponding to $E_{R,max}$ is about 7.5 for $\widetilde{W}_m = 0.5$ and increases to about 10 as $E_{R,max}$ grows asymptotically. At such high $\widetilde{W}_m$, the values of $\Lambda^*_{x,opt}$ are thus estimated to be about half of the ones in Table I.

3. Velocity and pressure profiles of the streaks

The velocity and pressure profiles of the Klebanoff modes are studied at $\bar{x} = 1.18$ for $\kappa_z = \kappa_y = 1$, $k_x = 0.1$, and $\hat{u}_3^{\infty} = -0.2$. The wall forcing conditions are $\widetilde{W}_m = 0.08,\ 0.16,$ and 0.32 and $\mathcal{K}_x = 2$. The full streak solution (7) is employed as it provides an accurate representation of the streak structures along the whole wall-normal extent of the boundary layer. It was found by R09 that the velocity component $\bar{u}^{(0)}$ becomes dominant in the outer part of the Blasius layer where $\bar{u}$ vanishes, although it is of second-order importance in the core of the boundary layer.

Figures 9 and 10 show that the streamwise velocity is attenuated the most. This is a noteworthy result as this velocity component is asymptotically larger than the wall-normal and the spanwise velocity components. The peak values of $|\bar{u}_0|$ and $|\bar{v}_0|$ shift toward the free stream, and the wall-shear stress produced by all the velocity components is reduced significantly. The profile of the spanwise velocity shows a more gradual growth from the wall toward the free stream under forcing conditions. The pressure fluctuations at the wall are reduced by more than half of the fixed-wall value but they are slightly amplified in the outer part of the boundary layer for these $\widetilde{W}_m$ values.

IV. SUMMARY

The effects of steady spanwise wall oscillations beneath a Blasius boundary layer perturbed by free-stream vortical structures have been studied numerically. The wall forcing leaves the mean streamwise flow unchanged, but generates a spanwise viscous layer which is thinner than the Blasius layer. The asymptotic scaling analysis and the numerical results show that the spanwise boundary layer grows as $\Lambda_x^{*1/3}$, where Λ_x^* is the forcing wavelength, and downstream as $x^{*1/6}$. An analytical solution is found at large downstream distances.

The wall oscillation enhances the streak intensity when the streak spanwise wavelength is much larger than the Blasius boundary layer thickness, and attenuates it when these two quantities are comparable. As the latter scenario is commonly encountered in experimental investigations, the wall forcing is predicted to be an effective vehicle for the attenuation of full-spectrum Klebanoff modes. Amongst the three velocity components, the streamwise velocity is the most affected one, which portends favourably for practical applications because this is the dominant velocity component within the boundary layer.

The asymptotic analysis reveals that order-one changes of the streak amplitude can be induced by a wall forcing amplitude which is an order of magnitude smaller than the free-stream velocity. This result is confirmed by the numerical calculations. Forcing amplitudes ten times smaller than the free-stream mean velocity can reduce the streak kinetic energy by 30%, and five times smaller can reduce the energy by half. Reductions of turbulence kinetic energy of the same amount are obtained with much higher forcing amplitudes, i.e. of comparable magnitude of the free-stream mean velocity for open boundary layers[4] or of the centreline velocity for channel flows.[7] Controlling the boundary layer by spanwise forcing during the pre-transitional stage is therefore likely to be more advantageous in energetic terms than during the fully developed turbulent regime. An optimal wavelength for maximum streak reduction is found and the values of such quantity for available laboratory data are estimated.

An experimental investigation of the flow studied herein will undoubtedly be a challenging task. As suggested by Wu,[34] a single three-dimensional vortical gust may be engendered by a thin vibrating wire positioned in the free stream parallel to the flat plate and at an angle with respect to the mean flow direction. A detailed description of such an apparatus for two-dimensional gusts is found in Dietz.[35] More complex free-stream vortical flows with specified spectral properties would be even more difficult to implement. A combination of rotating sinusoidal thin wires or the recently proposed fractal grids[36] may offer more controlled environments than the evenly spaced grids usually employed to generate the free-stream turbulence. Near-wall spanwise forcing could be generated by Lorentz-force actuation,[37] or by plasma actuators, as successfully done by Grundmann and Tropea[38] to attenuate the growth of Tollmien-Schlichting waves and by Hanson *et al.*[39] to damp transiently growing disturbances produced by wall roughness elements.

1. W. J. Jung, N. Mangiavacchi, and R. Akhavan, "Suppression of turbulence in wall-bounded flows by high-frequency spanwise oscillations," Phys. Fluids **4**(8), 1605 (1992).
2. F. Laadhari, L. Skandaji, and R. Morel, "Turbulence reduction in a boundary layer by local spanwise oscillating surface," Phys. Fluids **6**(10), 3218 (1994).
3. K.-S. Choi, "Near-wall structure of turbulent boundary layer with spanwise-wall oscillation," Phys. Fluids **14**(7), 2530 (2002).
4. P. Ricco and S. Wu, "On the effects of lateral wall oscillations on a turbulent boundary layer," Exp. Therm. Fluid Sci. **29**(1), 41 (2004).
5. J.-I. Choi, C.-X. Xu, and H. J. Sung, "Drag reduction by spanwise wall oscillation in wall-bounded turbulent flows," AIAA J. **40**(5), 842 (2002).
6. P. Ricco, "Modification of near-wall turbulence due to spanwise wall oscillations," J. Turbul. **5**(024), 1 (2004).
7. M. Quadrio and P. Ricco, "Critical assessment of turbulent drag reduction through spanwise wall oscillations," J. Fluid Mech. **521**, 251 (2004).
8. C. Viotti, M. Quadrio, and P. Luchini, "Streamwise oscillation of spanwise velocity at the wall of a channel for turbulent drag reduction," Phys. Fluids **21**, 115109 (2009).
9. M. Quadrio, P. Ricco, and C. Viotti, "Streamwise-travelling waves of spanwise wall velocity for turbulent drag reduction," J. Fluid Mech. **627**, 161 (2009).
10. F. Auteri, A. Baron, M. Belan, G. Campanardi, and M. Quadrio, "Experimental assessment of turbulent drag reduction by traveling waves in a turbulent pipe flow," Phys. Fluids **22**, 115103 (2010).
11. M. Quadrio and P. Ricco, "The laminar generalized Stokes layer and turbulent drag reduction," J. Fluid Mech. **667**, 135 (2011).
12. I. Galionis and P. Hall, "On the stabilization of the most amplified Görtler vortex on a concave surface by spanwise oscillations," J. Fluid Mech. **527**, 265 (2005).
13. P. J. Schmid and D. S. Henningson, *Stability and Transition in Shear Flows*, Applied Mathematical Sciences Vol. 142 (Springer, New York, 2001).
14. S. J. Leib, D. W. Wundrow, and M. E. Goldstein, "Effect of free-stream turbulence and other vortical disturbances on a laminar boundary layer," J. Fluid Mech. **380**, 169 (1999).
15. M. Matsubara and P. H. Alfredsson, "Disturbance growth in boundary layers subjected to free-stream turbulence," J. Fluid Mech. **430**, 149 (2001).
16. R. G. Jacobs and P. A. Durbin, "Simulations of bypass transition," J. Fluid Mech. **428**, 185 (2001).
17. X. Wu and M. Choudhari, "Linear and non-linear instabilities of a Blasius boundary layer perturbed by streamwise vortices. Part 2. Intermittent

instability induced by long-wavelength Klebanoff modes," J. Fluid Mech. **483**, 249 (2003).
[18]L. Brandt, "Numerical studies of the instability and breakdown of a boundary-layer low-speed streak," Eur. J. Mech. B/Fluids **26**(1), 64 (2007).
[19]S. Yoshioka, J. H. M. Fransson, and P. Alfredsson, "Free stream turbulence induced disturbances in boundary layers with wall suction," Phys. Fluids **16**(10), 3530 (2004).
[20]P. Ricco and F. Dilib, "The influence of wall suction and blowing on laminar boundary-layer streaks generated by free-stream vortical disturbances," Phys. Fluids **22**, 044101 (2010).
[21]P. Ricco, D. L. Tran, and G. Ye, "Wall heat transfer effects on Klebanoff modes and Tollmien-Schlichting waves in a compressible boundary layer," Phys. Fluids **21**, 024106 (2009).
[22]J.-C. Huang and M. W. Johnson, "The influence of compliant surfaces on bypass transition," Exp. Fluids **42**, 711 (2007).
[23]P. Ricco, "The pre-transitional Klebanoff modes and other boundary-layer disturbances induced by small-wavelength free-stream vorticity," J. Fluid Mech. **638**, 267 (2009).
[24]G. K. Batchelor, *An Introduction to Fluid Dynamics* (Cambridge University Press, London, 1967).
[25]T. Cebeci, *Convective Heat Transfer* (Springer-Verlag, Berlin, 2002).
[26]A. N. Gulyaev, V. E. Kozlov, V. R. Kuzenetsov, B. I. Mineev, and A. N. Sekundov, "Interaction of a laminar boundary layer with external turbulence," Fluid Dyn. **24**(5), 700 (1989).
[27]M. Abramowitz and I. A. Stegun, "Handbook of Mathematical Functions" (Dover, New York, 1965).
[28]K. J. A. Westin, A. V. Boiko, B. G. B. Klingmann, V. V. Kozlov, and P. H. Alfredsson, "Experiments in a boundary layer subjected to free stream turbulence. Part 1. Boundary layer structure and receptivity," J. Fluid Mech. **281**, 193 (1994).
[29]J. H. Watmuff, "Detrimental effects of almost immeasurably small free stream nonuniformities generated by wind-tunnel screens," AIAA J. **36**(3), 379 (1998).
[30]A. Inasawa, F. Lundell, M. Matsubara, Y. Kohama, and P. H. Alfredsson, "Velocity statistics and flow structures observed in bypass transition using stereo PTV," Exp. Fluids **34**, 242 (2003).
[31]J. Mans, E. C. Kadijk, H. C. de Lange, and A. A. van Steenhoven, "Breakdown in a boundary layer exposed to free-stream turbulence," Exp. Fluids **39**, 1071 (2005).
[32]J. Mans, H. C. de Lange, and A. A. van Steenhoven, "Sinuous breakdown in a flat plate boundary layer exposed to free-stream turbulence," Phys. Fluids **19**, 088101 (2007).
[33]S. V. Zhigulev, A. A. Uspenskii, and M. V. Ustinov, "Effect of the free-stream turbulence scale and the leading edge shape on boundary layer laminar-turbulent transition," Fluid Dyn. **44**(1), 31 (2009).
[34]X. Wu, "Receptivity of boundary layers with distributed roughness to vortical and acoustic disturbances: A second-order asymptotic theory and comparison with experiments," J. Fluid Mech. **431**, 91 (2001).
[35]A. J. Dietz, "Local boundary-layer receptivity to a convected free-stream disturbance," J. Fluid Mech. **378**, 291 (1999).
[36]D. Hurst and J. C. Vassilicos, "Scaling and decay of fractal-generated turbulence," Phys. Fluids **19**(3), 035103 (2007).
[37]J. Pang and K.-S. Choi, "Turbulent drag reduction by Lorentz force oscillation," Phys. Fluids **16**(5), L35 (2004).
[38]S. Grundmann and C. Tropea, "Active cancellation of artificially introduced Tollmien-Schlicting waves using plasma actuators," Exp. Fluids **44**(5), 795 (2008).
[39]R. E. Hanson, P. Lavoie, A. M. Naguib, and J. F. Morrison, "Transient growth instability cancelation by a plasma actuator array," Exp. Fluids **49**(6), 1339 (2010).